

Domain-wall excitations and optical conductivity in one-dimensional Wigner lattices

Matthias Mayr* and Peter Horsch

Max-Planck-Institut für Festkörperforschung, Heisenbergstrasse 1, D-70569 Stuttgart, Germany

(Received 17 January 2006; revised manuscript received 23 March 2006; published 2 May 2006)

Motivated by the recent finding that doped edge-sharing Cu-O chain compounds such as $\text{Na}_3\text{Cu}_2\text{O}_4$ and $\text{Na}_8\text{Cu}_5\text{O}_{10}$ are realizations of one-dimensional (1D) Wigner crystals, we study the optical spectra of such systems. Charge excitations in 1D Wigner crystals are described in terms of domain-wall excitations with fractional charge. We investigate analytically and numerically the domain-wall excitations that dominate the optical absorption, and analyze the dispersion and the parameter range of exciton states characteristic for the long-ranged Coulomb attraction between domain walls. Here we focus on the Wigner lattice at quarter-filling relevant for $\text{Na}_3\text{Cu}_2\text{O}_4$ and analyze, in particular, the role of second-neighbor hopping t_2 which is important in edge-sharing chain compounds. Large t_2 drives an instability of the Wigner lattice via a soft domain-wall exciton towards a charge-density wave with a modulation period distinct from that of the Wigner lattice. Furthermore we calculate the temperature dependence of the dc conductivity and show that it can be described by activated behavior combined with a $T^{-\alpha}$ dependent mobility.

DOI: [10.1103/PhysRevB.73.195103](https://doi.org/10.1103/PhysRevB.73.195103)

PACS number(s): 71.10.Fd, 78.20.Bh, 73.20.Qt, 71.35.-y

I. INTRODUCTION

At very low density an electron gas is expected to crystallize and to form a Wigner crystal, as in this limit the Coulomb interaction among electrons dominates their kinetic energy.¹ In the 1970s Hubbard² as well as Kondo and Yamaji³ suggested, expanding the considerations by Wigner, that the distribution of electrons in certain tetracyanoquinodimethane (TCNQ) charge transfer salts may be controlled rather by the Coulomb interaction than by the kinetic energy (\sim bandwidth), such that the electrons form a *generalized* Wigner lattice (WL) on the underlying TCNQ chain structure. This view suggests a strikingly different nature of charge excitations namely domain walls with fractional charge rather than particle-hole excitations as in usual metals and semiconductors.² This proposal, however, may be challenged on the grounds that the resulting periodicity of charge modulation can alternatively be explained by a $4k_F$ charge-density wave (CDW) (Refs. 4–6) arising from an instability of the Fermi surface even in models with *short-range* interactions. In fact, there is only a gradual crossover between the WL and the $4k_F$ CDW, thus there is no clear distinction between the two on the basis of the charge modulation period possible.⁷

In a recent study⁸ of a new class of charge-ordered compounds $\text{Na}_{1+x}\text{CuO}_2$,⁹ which contain edge-sharing Cu-O chains, it has been suggested that the magnetic and thermodynamic properties of these compounds can only be explained in terms of WL formation. Edge-sharing chains consist of CuO_4 squares just like the Cu-O planes of high- T_c cuprates, but they are differently linked. The edge-sharing arrangement of CuO_4 squares meets the WL criterion of small bandwidth in an optimal way due to the almost 90° Cu-O-Cu bonds (Fig. 1). Unexpected complexity is added because, apart from a small nearest-neighbor-hopping matrix element t_1 , the second-neighbor hopping t_2 has to be considered which turns out larger as a consequence of the structure. While this unusual feature does not affect the classical WL order imposed by the Coulomb interaction, it changes the

Fermi surface topology,¹⁰ and thereby allows us to distinguish the WL from the CDW on the basis of the modulation period. The $\text{Na}_{1+x}\text{CuO}_2$ compounds thus provide a first example where an unambiguous distinction between the generalized WL and a Fermi surface related CDW is possible.

The electron interaction driven $4k_F$ CDW has to be distinguished from the more familiar $2k_F$ Peierls instability which arises from a modulation of hopping matrix elements due to the coupling to periodic lattice distortions, i.e., leading to a CDW centered on bonds rather than on the ions.¹¹ In contrast the Wigner lattice is based not on quantum but on classical energy considerations, namely which distribution of localized electrons has the lowest Coulomb interaction. It is quite remarkable though, that the periodicity of the WL coincides with that of the $4k_F$ CDW which emerges from a Fermi surface instability, i.e., from a pure quantum mechanical effect of strongly correlated electrons in models with nearest-neighbor hopping.

Strictly speaking, at finite hopping t_l ($l=1, 2, \dots$) the generalized WL is a *quantum solid*.^{12,13} The kinetic energy causes virtual transitions to neighbor sites and leads thereby to a quantum mechanical smearing of the electron positions. Hence electrons should be rather visualized as electron clouds that form a WL as consequence of the long-range

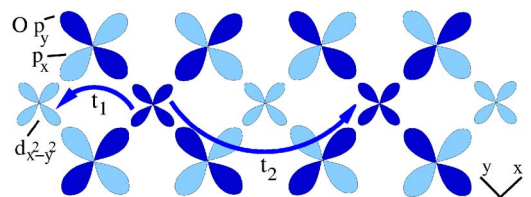


FIG. 1. (Color online) Orbital structure of edge-sharing copper-oxygen chains. The 90° Cu-O-Cu hopping t_1 and the second-neighbor Cu-O-O-Cu hopping path t_2 are marked by arrows. Shading indicates the p - d covalent mixing, as well as the hole distribution in the $d^9 L_h$ Zhang-Rice singlet states in $\text{Na}_3\text{Cu}_2\text{O}_4$ with an alternating charge order (dark shading).

Coulomb interaction. This delocalization of the electron in the WL is a pure quantum effect, i.e., controlled by the interplay of kinetic and interaction energies. The quantum mechanical blurring of the electron position has considerable effects on the physical properties of Wigner lattices, as discussed in Ref. 8 in the context of edge-sharing chains in $\text{Na}_3\text{Cu}_2\text{O}_4$ and $\text{Na}_8\text{Cu}_5\text{O}_{10}$ compounds, where superexchange interactions and thereby the magnetic properties are strongly influenced by the quantum nature of the WL.

The aim of the present paper is to explore the charge excitations of the one-dimensional (1D) WL, which are characterized as domain-wall excitations. We calculated the optical conductivity and its temperature dependence, as it is hoped that forthcoming experiments may provide further evidence for the WL nature of the electron structure of the $\text{Na}_{1+x}\text{CuO}_2$ edge-sharing chain compounds. We use here both numerical, i.e., zero and finite-temperature diagonalization, and analytical methods to arrive at a deeper understanding of the nature of charge excitations in 1D Wigner lattices at quarter filling. In particular, we find that the long-range (repulsive) Coulomb interaction among electrons leads to exciton states below the domain-wall continuum, which appear as strong exciton absorptions in the optical conductivity in the case of small hopping t_1 . Remarkably the second-neighbor-hopping processes t_2 are found to contribute strongly to the exciton dispersion. These processes lift the degeneracy of the exciton state and the lower branch gets soft at momentum $q = \pi/2$ and leads to an exciton instability at a critical value $t_{2,c}$. The CDW state beyond $t_{2,c}$ has a modulation period twice as large as that of the WL. Calculations of the static structure factor show that the charge modulation in the CDW state is weak compared to the WL state. Finally, we have calculated the temperature dependence of the dc conductivity $\sigma(T)$ of the generalized Wigner lattice. The data for $\sigma(T)$ determined from the low-frequency absorption show a crossover from an activated behavior at low temperature to a weak (poor metal-like) temperature dependence above the melting temperature of the WL.

Doped edge-sharing chains are also building blocks of the intensively studied system $\text{Sr}_{14-x}\text{Ca}_x\text{Cu}_{24}\text{O}_{41}$, the so-called telephone number compounds.^{14–16} The composite structure of these materials consists of both ladder and chain structures.¹⁷ While originally the attention was directed toward the electronic properties of the ladders, because of their structural similarity to the high- T_c cuprates,¹⁸ more recently the number of papers reporting information concerning the chains is increasing. The magnetic properties of these compounds, which depend strongly on the doping, are usually attributed to the chains.^{19–21} Recently, a quintupling of the chain unit cell in $\text{Sr}_{14}\text{Cu}_{24}\text{O}_{41}$ due to a charge ordering below ~ 200 K was reported.^{22,23} An additional complexity of these compounds is due to the exchange of holes between chains and ladders,¹⁵ i.e., the doping concentration of edge-sharing chains is difficult to infer precisely. Moreover, an incommensurate modulation results from a misfit between the unit cells of ladders and chains. Work by van Smaalen²⁴ and particularly a neutron scattering study of Braden *et al.*²⁵ illuminate the subtle aspects of the interplay between modulations of chains and ladders. It has also been argued that the misfit between chains and ladders may modify the charge ordering

and hence the spin structure on the chains.²⁶ Particularly remarkable is a study by Isobe *et al.*,²⁷ who succeeded in resolving the internal charge structure of the charge modulation of the compound $[(\text{Sr}_{0.029}\text{Ca}_{0.971})_2\text{Cu}_2\text{O}_3]_{54}[\text{Cu O}_2]_{77}$ with a chain unit cell containing 77 Cu sites. An inspection shows that the charge pattern found in the structure analysis compares favorably with that expected for a generalized Wigner lattice. Recently also the modulation of the charge density in the ladders of $\text{Sr}_{14}\text{Cu}_{24}\text{O}_{41}$ has been reported by Abbamonte *et al.*²⁸

Wigner crystals are prime examples for strongly correlated states in the sense that electrons do the utmost to avoid each other in real space.²⁹ In general, strong correlations (i.e., large on-site interaction U) and the associated reduction of the kinetic energy are favorable for charge localization. As a consequence the long-range Coulomb interaction may become relevant in strongly correlated systems, i.e., leading to charge-ordered states and WL order in higher dimensions at particular fillings. Examples are the manganites at quarter-filling which reveal checker-board charge order^{30,31} and the layered molecular crystals of the BEDT-TTF type.^{32–35} Also charge stripes in high- T_c compounds at $\frac{1}{8}$ doping³⁶ reflect the interplay of strong correlations and long-range Coulomb interactions.

The outline of the paper is as follows: In Sec. II we describe the Hubbard-Wigner model for edge-sharing chain systems and introduce the corresponding spinless fermion Hamiltonian. Furthermore we analyze the resulting domain-wall interactions for both Coulomb and truncated interactions. In Sec. III we present diagonalization results for the charge-excitation spectrum and analyze the emerging excitonic states in the case of the model with Coulomb interaction and nearest-neighbor hopping. Here we also provide an analytical derivation both for the continuum and the exciton states. The temperature dependence of the structure factor, kinetic energy, and optical conductivity are calculated by means of exact diagonalization (ED). Section IV deals with the significant changes of the excitonic states introduced by second-neighbor hopping. These are analyzed with help of the analytical solution. In particular, we show here that the soft exciton states near $q = \pi/2$ are visible in the optical conductivity at elevated temperature as midgap absorption. Finally the dc conductivity of 1D Wigner lattices is discussed in Sec. V, while our conclusions are summarized in Sec. VI.

II. MODEL

A. Wigner lattices in doped edge-sharing chain compounds

As in the high- T_c cuprates Cu^{2+} is in a d^9 configuration with spin $\frac{1}{2}$, while Cu^{3+} is in a d^9 -ligand hole (d^9L_h) singlet state, where the additional hole resides largely at the O neighbors of the Cu ion. This nonmagnetic configuration is also known as Zhang-Rice singlet.³⁷ In contrast to the high- T_c superconductors the edge-sharing geometry with nearly 90° Cu-O-Cu bonds (Fig. 1) leads to strongly reduced hopping matrix elements. This sets the stage for the long-range Coulomb force as a predominant interaction

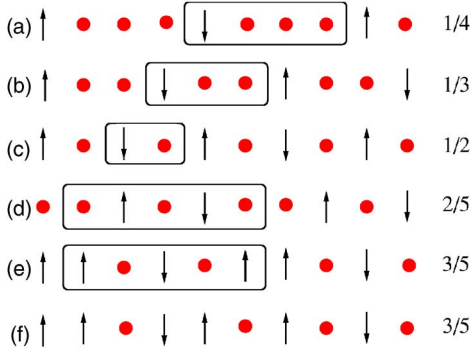


FIG. 2. (Color online) Wigner charge order resulting from Coulomb repulsion and the associated modulated Heisenberg spin structure for various concentrations $\rho = \frac{1}{4}, \frac{1}{3}, \frac{1}{2}, \frac{2}{5}$, and $\frac{3}{5}$ (a)–(e). The spin- $\frac{1}{2}$ of Cu^{2+} (arrows) is responsible for magnetism, whereas Cu^{3+} (circle) is nonmagnetic. The spin arrangement is that expected for ferromagnetic J_1 and antiferromagnetic J_2 exchange interactions. The charge unit cells (shaded) contain 4, 3, 2, and 5 sites, respectively. The structures (c) and (e) are realized in $\text{Na}_3\text{Cu}_2\text{O}_4$ and $\text{Na}_8\text{Cu}_5\text{O}_{10}$, respectively. A fluctuation of spin position due to a low-energy charge excitation is shown in (f) for $\rho = \frac{3}{5}$.

$$H_{Coul} = U \sum_i n_{i,\uparrow} n_{i,\downarrow} + \sum_{i,l \geq 1} V_l n_i n_{i+l}, \quad (1)$$

where the on-site interaction U takes care of the strongly correlated character of these systems and suppresses charge fluctuations leading to Cu^{1+} (d^{10}) configurations. In our model we associate the $d^9 L_h$ (d^9, d^{10}) ionization state with 0 (1,2) electrons, respectively, and $n_{i,\sigma}$ ($\sigma = \uparrow, \downarrow$) counts the number of electrons with spin σ , while $n_i = n_{i,\uparrow} + n_{i,\downarrow}$. Thus the concentration of electrons ρ is related to the concentration of holes $\delta = 1 - \rho$ (relative to the d^9 configuration) used in the high- T_c literature.³⁸ The Coulomb interaction V_l is screened by the polarization of neighboring chains and by core electrons.² We shall not try to explore the subtleties of screening due to the embedding, and assume for the sake of simplicity a generic Coulomb law $V_l = \frac{V}{l}$, $l = 1, 2, \dots$, and keep the nearest-neighbor interaction V as a parameter.³⁹ It is crucial for the following that the interaction is long ranged and convex, i.e., $V'_l = V_{l-1} - 2V_l + V_{l+1} > 0$.

For a commensurate doping concentration $\rho = m/n$ the interaction V_l selects a particular charge-ordering pattern.² The resulting charge order is immediately obvious for the filling fractions $\rho = \frac{1}{4}, \frac{1}{3}$, and $\frac{1}{2}$ [Figs. 2(a)–2(c)], which involve an equidistant arrangement of the Cu^{2+} sites (arrows in Fig. 2). For a general ratio $\rho = m/n$ this leads to complex structures with unit cell size n . In case of $\rho = \frac{2}{5}$ and $\frac{3}{5}$ we encounter in Figs. 2(d) and 2(e) the charge order observed for $\text{Sr}_{14}\text{Cu}_{24}\text{O}_{41}$ (Refs. 22 and 23) and $\text{Na}_8\text{Cu}_5\text{O}_{10}$,⁸ respectively. Charge localization, however, is not perfect in Wigner insulators as electrons still undergo virtual transitions to neighboring sites [Fig. 2(f)] in order to retain partially their *kinetic energy*. The energy of the lowest excitations and the impact of kinetic energy depend strongly on $\rho = m/n$. For example, the energy of the lowest excitation relative to the ground state Fig. 2(c) is $\sim V''_5$ while the excitation for $\rho = \frac{3}{5}$ shown in Fig. 2(f) is

$\sim V''_5$, about an order of magnitude smaller. Hence quantum charge fluctuations are more important in the latter case.⁸

To investigate the role of kinetic energy we explore the dynamics of electrons starting from the one-dimensional *Hubbard-Wigner model* $H_{HW} = H_{Coul} + H_{Kin}$,² where

$$H_{Kin} = - \sum_{i,l,\sigma} t_l (c_{i+l,\sigma}^\dagger c_{i,\sigma} + c_{i,\sigma}^\dagger c_{i+l,\sigma}) \quad (2)$$

describes the hopping of an electron with spin σ from site i to site $i+l$ and vice versa; and $n_{i,\sigma} = c_{i,\sigma}^\dagger c_{i,\sigma}$. Due to the almost 90° Cu-O-Cu angle the hopping t_1 between nearest-neighbor Cu sites results mainly from direct d - d exchange, while t_2 originates from hopping via a Cu-O-O-Cu path⁴⁰ (Fig. 1), leading to the remarkable fact $|t_2| > |t_1|$. We adopt here as typical values $t_1 \sim 63$ meV, $t_2 \sim 94$ meV, derived from *ab initio* band structure calculations for the Cu^{2+} edge-sharing reference system Li_2CuO_2 .⁴¹ The hopping integrals are much smaller than our estimates⁸ for $U \sim 3.8$ eV and $V \sim 1.5$ eV. Thus these parameters suggest that the edge-sharing chain compounds are well inside the WL regime.

In particular $|t_2| > |t_1|$ implies that the second-neighbor (antiferromagnetic) exchange integral J_2 is large compared to the nearest-neighbor interaction J_1 and the interchain couplings. In fact, this is consistent with the magnetic properties of the $\text{Na}_3\text{Cu}_2\text{O}_4$ and $\text{Na}_8\text{Cu}_5\text{O}_{10}$ compounds⁸ and also with recent neutron diffraction data of the compound NaCu_2O_2 which consists of $\rho = 1$ edge-sharing chains.⁴² Magnetic excitation spectra determined by Raman spectroscopy⁴³ and a high-field NMR study⁴⁴ on NaCu_2O_2 single crystals confirm these conclusions.

It is evident that the spatial variation of charges in the WL at the same time implies a complementary arrangement for the spins and thus leads to *spatially modulated Heisenberg spin chains* with varying distances among the spins.^{8,45} This new category of spin models shows very different magnetic properties for different commensurabilities $\rho = m/n$, as actually observed in the $\text{Sr}_{14-x}\text{Ca}_x\text{Cu}_{24}\text{O}_{41}$ compounds^{20,21} and in the $\text{Na}_{1+x}\text{CuO}_2$ systems. For example, $\text{Sr}_{14}\text{Cu}_{24}\text{O}_{41}$ has the commensurability $\rho = \frac{2}{5}$ corresponding to the structure shown in Fig. 2(d) and its ground state is determined by singlet pairs.^{22,23,46,47} Thus its magnetic properties are quite distinct from those of $\text{Na}_3\text{Cu}_2\text{O}_4$ ($\rho = \frac{1}{2}$) and $\text{Na}_8\text{Cu}_5\text{O}_{10}$ ($\rho = \frac{3}{5}$).⁸

B. Spinless fermions and domain-wall interaction

Our study of the charge structure and dynamics will be based on the spinless fermion version of the Hubbard-Wigner Hamiltonian $H = H_t + H_C$:

$$H = - \sum_{i,l \geq 1} t_l (c_i^\dagger c_{i+l} + c_{i+l}^\dagger c_i) + \sum_{i,l \geq 1} V_l n_i n_{i+l}. \quad (3)$$

The underlying assumption of spin-charge separation, i.e., the neglect of the effects of spin degrees of freedom on charge correlations and excitations, can be rationalized when starting from the 1D Hubbard model which is Bethe ansatz soluble.⁴⁸ That model has marginal spin-charge coupling^{49–52} and its charge excitations can be described by free spinless fermions.⁵³ The addition of the long-range Coulomb interaction leads then to the model of interacting spinless fermions

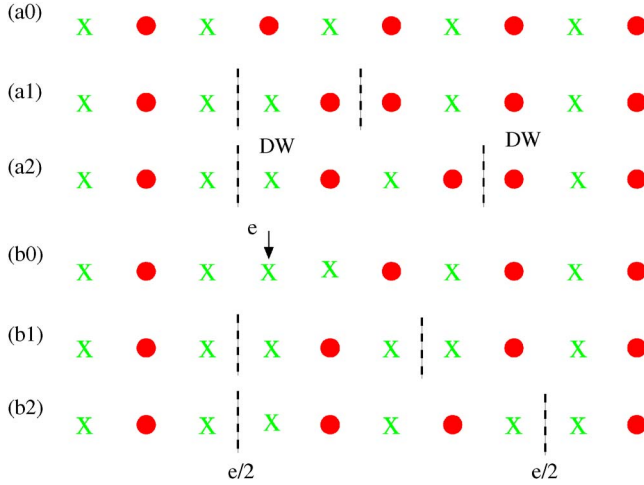


FIG. 3. (Color online) (a) Charge excitations in a Wigner lattice move in the form of domain walls (DW's). Here we consider the $\rho=0.5$ case where Cu^{2+} (Cu^{3+}) are indicated by x (\bullet), respectively. (b) The addition of an extra electron with charge e leads to a high-energy state which decays into two DW's with a fractional charge $e/2$.

which may be used to investigate the charge structure and dynamics of WL's. We note, however, that strictly speaking in the 1D Hubbard-Wigner model there is some coupling between charge and spin, i.e., resulting from the long-range Coulomb interaction. For example, quantum charge fluctuations influence exchange interactions and thereby the magnetic response of WL's as discussed in Ref. 8. Such coupling effects between spin and charge will be neglected here.

In the following we shall focus on the $\rho=\frac{1}{2}$ case. The ground state has perfect alternating charge order as shown in Fig. 3(a0) for $t_1=0$. At finite hopping t_1 this ground state remains stable, yet domain-wall pairs get mixed in due to quantum fluctuations. An elementary t_1 hopping process involves the interchange of $(x0) \rightarrow (0x)$ pairs in Fig. 3. The charge excitations in Wigner lattices, caused, e.g., by optical excitations, involve the creation of domain-wall (DW) pairs. These DW's can move as a consequence of t_1 processes of the kinetic energy. The role of t_2 processes is distinct in the $\rho=\frac{1}{2}$ case; they are blocked in the perfect WL and contribute only in the presence of DW pairs. We shall consider this problem in a later section, and assume for the moment $t_2=0$.

The charge of a DW can be invoked from a Gedanken experiment due to Hubbard.² The excitation generated by adding an extra electron with charge e as shown in Fig. 3(b0) will dissociate into two equivalent DW's with a fractional charge $e/2$ separated by regions of perfect charge order. In general, the domain-wall charge depends on the commensurability $\rho=m/n$.

The creation of a domain-wall pair requires an energy $\propto V_1$. Domain walls can propagate freely, yet due to the long-range interaction V_l they attract each other. For $\rho=\frac{1}{2}$ the energy of two domain walls Δ_m at distance $d=2m$ is determined by the recursion relation

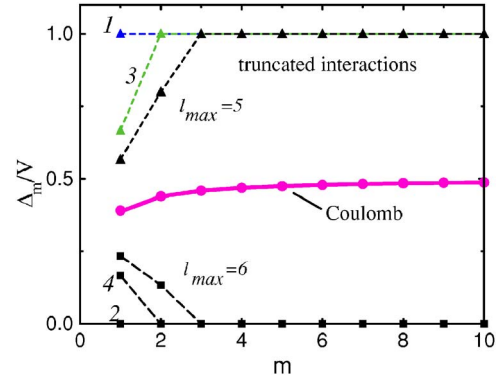


FIG. 4. (Color online) Interaction energy Δ_m of two DW's at a distance $d=2m$ for a Wigner lattice with density $\rho=0.5$. The result for the Coulomb interaction (solid line) and asymptotic expression (circles) is compared with Δ_m obtained for the Coulomb interaction truncated at $l_{max}=1, 2, \dots, 6$ (triangles and squares).

$$\Delta_m = \Delta_{m-1} + \sum_{n=m}^{\infty} V''_{2n}, \quad m = 2, 3, \dots, \quad (4)$$

with $\Delta_1 = \sum_{n=1}^{\infty} V''_{2n}$. Here $V'_l = V_{l-1} - 2V_l + V_{l+1}$ denotes the discrete second derivative of the interaction. In the following we shall assume the Coulomb interaction $V_l = V/l$, and furtheron use $V=1$ as unit of energy. In this case $\Delta_1 = 2 \ln 2 - 1$.

An excellent asymptotic expansion for the domain-wall interaction (DWI) has been derived by Fratini *et al.*⁵⁴ for the Coulomb case:

$$\Delta_m \approx \frac{1}{2} - 1/8m + 1/(4m)^3 - \dots \quad (5)$$

Remarkably this expression has an accuracy of two digits even at $m=1$. It is interesting to note that the leading interaction term $-1/8m$ in the asymptotic expansion can be interpreted in terms of an effective Coulomb interaction between the fractional charges of DW's $q_{1,2} = \pm 1/2$. That is, the DW interaction is given as $q_1 q_2 / d = -1/8m$, where $d=2m$ is the distance between the DW centers. Hence the interaction between the domain walls Δ_m provides a manifestation of the fractional charge of the domain walls.

It is evident that a truncated Coulomb interaction, i.e., $V_l=0$ for $l > l_{max}$, may not stabilize the Wigner lattice structure at general rational fillings.^{2,55,56} The required value for l_{max} increases with the commensurability n , where $\rho=m/n$ is the filling fraction. In the case of the excitations truncation is even worse. This problem is demonstrated in Fig. 4 which displays the energy Δ_m of two domain walls as function of distance $d=2m$ for the most simple Wigner lattice $\rho=\frac{1}{2}$. In the case of Coulomb interaction Δ_m is an increasing function of m , i.e., the domain-wall interaction is attractive, and converges against $\Delta_{\infty}=\frac{1}{2}$. Remarkably truncation leads to two different classes of behavior, repulsion at a short distance for $l_{max}=\text{even}$ and attraction for $l_{max}=\text{odd}$. Note that in the former case $\Delta_l \rightarrow 0$ for large l , while for $l_{max}=1$ which is sufficient to stabilize the Wigner lattice for $\rho=\frac{1}{2}$ there is neither attraction nor repulsion, i.e., DW pairs are not confined in this case. Hence, calculations of excitation spectra based on

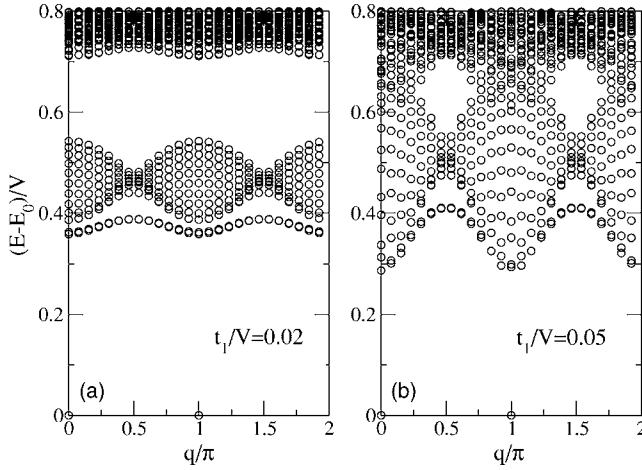


FIG. 5. Excitation spectrum for the quarter-filled chain with $N=26$ sites and Coulomb interaction ($V=1$) for (a) $t_1/V=0.02$ and (b) $t_1/V=0.05$ as obtained by exact diagonalization. The continuum due to domain-wall pairs is centered at $E \sim 0.45$ V and its width is $\sim 8t_1$. At small t_1 the bound state is well separated from the bottom of the continuum, while for larger t_1 (b) it merges with the continuum, but persists near $q=\pi/2$. Parts of a continuum due to an excitation of four domain walls is visible at the top of the figure.

models with truncated interaction $V_1, V_2, \dots, V_{l_{max}}$ or models with arbitrarily chosen parameters V_1, V_2 , etc. must be considered with care when they are compared to the Coulomb case. A frequently studied model is the model with both nearest-neighbor-hopping t_1 and nearest-neighbor interaction V_1 .^{5,57,58} The effects of longer-range interactions have been studied by Poilblanc *et al.*,⁵⁹ though for relatively weak interactions, i.e., outside the WL regime.

In this work we shall confine ourselves mainly to the discussion of the long-range Coulomb interaction. For the analytical considerations we shall occasionally consider the truncated models with $l_{max}=1$ and $l_{max}=3$.

III. RESULTS FOR NEAREST-NEIGHBOR HOPPING

A. Domain-wall continuum and exciton

As shown above charge excitations in Wigner lattices form domain walls (DW's) separating regions of perfect charge order. DW's move as a consequence of the kinetic energy operator H_t . For the sake of transparency we consider first the model with nearest-neighbor-hopping motion t_1 . Numerical results for the excitation spectra for the Coulomb interaction are given in Fig. 5 for a quarter-filled ring (i.e., $\rho=\frac{1}{2}$) with $N=26$ sites. The figure shows the two degenerate ground states at $q=0$ and π , the two domain-wall continuum and part of the four DW continuum at high energy. The two DW continuum is centered near $E \sim 0.45$ V as expected from the DW interaction $\Delta_m \approx \frac{1}{2} - 1/8m + 1/(4m)^3 - \dots$ in the Coulomb case. As a result of the Coulomb attraction between DW pairs an excitonic state emerges below the two DW continuum, which is expected to play a prominent role in the optical absorption. With increasing hopping t_1 the width

of the two DW spectrum $\sim 8t_1$ increases and the exciton binding energy decreases, and eventually the exciton is absorbed by the continuum near $q=0$ and π . Yet due to the dispersion of both the lower edge of the two DW continuum and the exciton, the excitonic state survives in the vicinity of $q=\pi/2$.

Next we explore the analytical structure of the DW continuum and then analyze the dispersion of the exciton in more detail. We will address three different problems: (i) The DW continuum in the case that all Δ_l are equal. This case pertains to the model where only the nearest-neighbor (NN) interaction V_1 is kept. There is no exciton state in this case and DW's are not confined.^{56,60} (ii) Next we explore the solution for the bound state emerging for $\Delta_1 < \Delta_\infty$ and $\Delta_l = \Delta_\infty$ for $l \geq 2$. This case directly applies to the model where the Coulomb interaction is truncated at $l_{max}=3$, but this solution also provides an approximate description for the case with the full Coulomb interaction, if one adopts appropriate values for Δ_1 and Δ_∞ . Finally (iii), we analyze the special role of the second-neighbor hopping t_2 in the case $\rho=\frac{1}{2}$.

We begin with the motion of a DW pair as indicated in Fig. 3(a) and denote the pair state by $|n, m\rangle$. Here $n-m$ and $n+m$ denote the centers of the xx and 00 DW's indicated by vertical bars in Fig. 3, while n denotes the center of mass coordinate of a DW pair. We shall consider periodic boundary conditions, that is, even numbered rings of size N . Then it is useful to introduce the auxiliary Bloch states

$$|\psi_{q,m}\rangle = \frac{1}{\sqrt{N}} \sum_n e^{iqn} |n, m\rangle; \quad (6)$$

where for periodic boundary conditions momenta are defined as $q_\nu = 2\pi\nu/N$ and $\nu=0, 1, \dots, N-1$. When applying the translational operator T_l one obtains $T_l |\psi_{q,m}\rangle = e^{-iq'l} |\psi_{q,m}\rangle$. The DW interaction energy associated with these states is Δ_m as discussed above:

$$H_C |\psi_{q,m}\rangle = \Delta_m |\psi_{q,m}\rangle. \quad (7)$$

The action of the kinetic energy operator H_t on the local DW states yields

$$H_t |n, m\rangle = t_1 [(|n-1, m+1\rangle + |n+1, m+1\rangle)(1 - \delta_{m+1, N/2}) + (|n+1, m-1\rangle + |n-1, m-1\rangle)(1 - \delta_{m-1, 0})]. \quad (8)$$

This can be expressed in terms of the auxiliary Bloch basis Eq. (6) as

$$H_t |\psi_{q,m}\rangle = t_1(q) [(1 - \delta_{m+1, N/2}) |\psi_{q, m+1}\rangle + (1 - \delta_{m-1, 0}) |\psi_{q, m-1}\rangle], \quad (9)$$

with $t_1(q) = 2t_1 \cos(q)$. (i) In the case where all Δ_m have the same value, which we denote Δ_∞ , the solution for the domain-wall continuum is straightforward:

$$|\Phi_{q,p}\rangle = \frac{2}{\sqrt{N}} \sum_{m=1}^{N/2-1} \sin(pm) |\psi_{q,m}\rangle, \quad (10)$$

where the $N/2-1$ pseudomomenta are determined by $p_\mu = 2\pi\mu/N$ and $\mu=1, 2, \dots, N/2-1$. The corresponding energies of the DW continuum are

$$E_{q,p} = \Delta_\infty + 2t_1[\cos(q+p) + \cos(q-p)]. \quad (11)$$

That is, they are given as linear combinations of single domain-wall energies. The total width of the continuum is $8t_1$.

While the t_1 - V_1 model with nearest-neighbor interaction stabilizes the alternating charge-ordered ground state for $\rho = 0.5$, it does not lead to an attractive interaction between domain walls. The excitation spectrum consists of the domain-wall continuum. The absence of the domain-wall exciton shows that domain walls are not confined in this case.^{56,60}

The simplest case which shows a bound state is the model where the Coulomb interaction is truncated at $l_{max}=3$. The resulting DWI Δ_m in this case is $\Delta_1 = \frac{2}{3}V$ and $\Delta_m = \Delta_\infty = V$ for $m \geq 2$, i.e., the DW continuum is centered around V . Next we shall derive an analytical expression for the exciton energy.

The exciton solution can be obtained by an expansion of the secular determinant

$$D = \begin{vmatrix} \omega_1 & t_1(q) & 0 & 0 & \dots & 0 \\ t_1(q) & \omega_2 & t_1(q) & 0 & \dots & 0 \\ 0 & t_1(q) & \omega_2 & t_1(q) & \dots & 0 \\ \vdots & \vdots & \vdots & \ddots & \vdots & \vdots \\ 0 & \dots & 0 & t_1(q) & \omega_2 & t_1(q) \\ 0 & \dots & 0 & 0 & t_1(q) & \omega_1 \end{vmatrix}, \quad (12)$$

where $\omega_l = \Delta_l - E$ and $t_1(q) = 2t_1 \cos(q)$.

$$D = \omega_1^2 D_M - 2\omega_1 t_1(q)^2 D_{M-1} + t_1(q)^4 D_{M-2}, \quad (13)$$

$$D_M = \begin{vmatrix} \omega_2 & t_1(q) & \dots & \dots \\ t_1(q) & \omega_2 & t_1(q) & \dots \\ \vdots & \vdots & \ddots & \vdots \\ \dots & \dots & t_1(q) & \omega_2 \end{vmatrix}, \quad (14)$$

$$D_M = \omega_2 D_{M-1} - t_1(q)^2 D_{M-2}, \quad (15)$$

where $D_1 = \omega_2$, $D_2 = \omega_2^2 - t_1(q)^2$, and $D_0 = 1$. The last relation is required so that the previous determinantal equation is fulfilled for $M \geq 2$. The equation may be solved by the polynomial ansatz $D_M = p^M$, leading to

$$p = \frac{1}{2} [\omega_2 \pm \sqrt{\omega_2^2 - 4t_1(q)^2}]. \quad (16)$$

The equation for the bound state $\omega_1 p = t_1(q)^2$ takes then the form

$$(\Delta_1 - E)[\Delta_2 - E \pm \sqrt{(\Delta_2 - E)^2 - 4t_1(q)^2}] = 2t_1(q)^2. \quad (17)$$

The physical solution, which is twofold degenerate because of Eq. (13), is

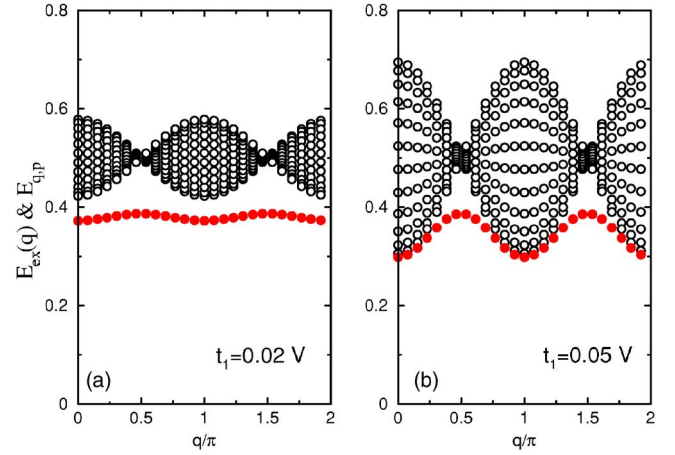


FIG. 6. (Color online) Analytical solution for the domain-wall continuum $E_{q,p}$, Eq. (11), of the quarter-filled chain with $N=26$ sites and $\Delta_m = \frac{1}{2}$ for $t_1=0.02$ and 0.05 . Data points (circles) representing the continuum are determined for the discrete momenta sets q_ν and p_μ . Exciton dispersion $E_{ex}(q)$, Eq. (18), calculated for the model with $\Delta_1 = 2 \ln 2 - 1$ and $\Delta_m = \frac{1}{2}$ for $m \geq 2$ relevant for the case of long-range interaction (filled circles).

$$E_{ex}(q) = \Delta_1 - \frac{t_1(q)^2}{\Delta_2 - \Delta_1}, \quad (18)$$

where the dispersion $t_1(q) = 2t_1 \cos(q)$, which appears squared, reflects the hopping of domain walls by two lattice units. We also notice that the dispersion is weighted by the DW binding potential $\Delta_2 - \Delta_1$. As this quantity is $V/3$ in the model with a truncated interaction ($l_{max}=3$), the dispersion of the exciton (not shown) is smaller than in the model with the Coulomb interaction.

It is instructive to compare the analytical results obtained so far with the numerical data obtained for the Coulomb interaction displayed in Fig. 5. We approximate Δ_m as follows $\Delta_1 = 2 \ln 2 - 1$ and $\Delta_m = \frac{1}{2}$ for $m \geq 2$. The results are shown in Fig. 6. Although the approximation used for the DWI Δ_m is rather crude, there is quite a good agreement with exact diagonalization.

B. Structure factor and melting of Wigner lattice

Wigner lattice order gets weakened with increasing kinetic energy $\sim t_1$. Yet in the model with only nearest-neighbor hopping there is a *gradual crossover* to the CDW with weaker charge order but the same modulation period,⁶¹ which is $q = \pi$ at $\rho = \frac{1}{2}$. This is the $2k_F$ CDW of spinless fermions, and corresponds to the $4k_F$ CDW (Refs. 5 and 6) if the spin is included in the model. The crossover from the WL to the CDW regime is reflected in the variation of the charge gaps at $q = \pi(0)$ displayed in Fig. 7(a) as function of t_1 . While the two gaps are almost equal in the WL regime at small t_1 , for larger t_1 the $q = \pi (=2k_F)$ charge gap controls the CDW state. In this figure one can also see that in the WL regime the charge gaps calculated numerically for a $N=26$ site cluster are well described by the perturbative expression,

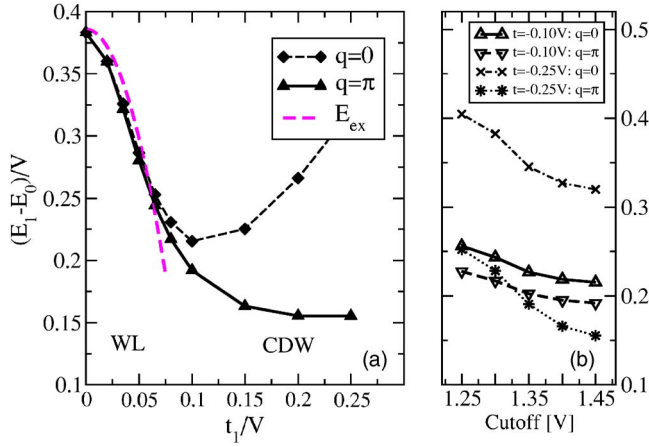


FIG. 7. (Color online) (a) The variation of the charge gap at $q=\pi$ as a function of t_1 displays the crossover from the Wigner lattice to the CDW regime in the case with the nearest-neighbor hopping t_1 . Results are obtained for an $N=26$ site ring using an energy cutoff 1.45 V. The exciton energy of WL (dashed curve) according to Eq. (18). (b) Dependence of the gap energies for large $t_1=0.1$ (0.25) on the cutoff energy.

Eq. (18), for the exciton energy E_{ex} using $\Delta_1=2 \ln 2 - 1$ and $\Delta_2=\frac{1}{2}$ appropriate for the WL stabilized by Coulomb interaction. We note, that for the model with the nearest-neighbor interaction V the CDW solution for $\rho=\frac{1}{2}$ is expected to be stable up to $t_1=0.5$ V,⁵⁸ at even higher values for t_1 a metallic state will be realized.⁵⁹

Next we shall investigate the disappearance of WL order due to thermal fluctuations. It is well known that one-dimensional systems controlled by short-range interactions do not exhibit long-range order at finite temperature. The corresponding absence of a phase transition at finite temperature follows from the Mermin-Wagner theorem.^{62,63} However, there is a *finite* transition temperature even in 1D models if the decay of interactions is power-law-like and sufficiently slow, as has been shown for Heisenberg and Ising systems with ferromagnetic⁶⁴ and antiferromagnetic⁶⁵ interactions. The latter work by Erwin and Hellberg, which deals with an interaction decaying as $1/R$, is of direct relevance for the WL case.

The melting of the generalized WL (Ref. 66) due to domain-wall excitations is reflected in the structure factor $N(q)$, whose temperature dependence we study here. The $T=0$ charge structure factor

$$N(q) = (1/N_e^2) \sum_{i,j} \exp^{iq(i-j)} \langle n_i n_j \rangle \quad (19)$$

is normalized here with respect to the total electron number of electrons N_e , such that $N(q=\pi)=1$ for perfect CO, that is, at low temperature and for small t_1 . The alternating charge order is reflected in the peak of $N(q)$ at $q=\pi$ which starts to decrease strongly for $T>0.05$ V. Yet even at much higher temperatures $N(q)$ reveals a maximum at $q=\pi$ which indicates the persistence of pronounced short-range charge correlations. The results for $N(\pi)$ displayed in the inset in Fig. 8 indicate the melting of Wigner charge order⁶⁷ at a tempera-

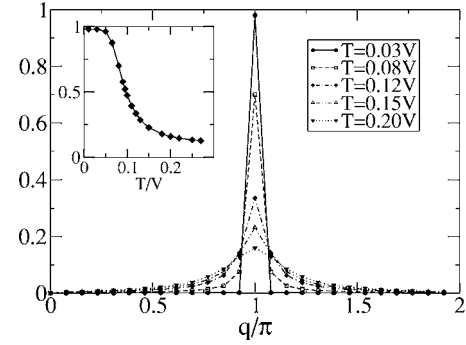


FIG. 8. Structure factor $N(q)$ versus q for a $N=26$ chain with Coulomb interaction and $t_1=0.02$ V for different temperatures. The inset shows the temperature dependence of $N(q=\pi)$.

ture $T_m \sim 0.06$ V, i.e., for the case of Coulomb interaction and $t_1=0.02$ V.

We note that $T_m \sim 0.06$ V ($V \sim 1$ eV) has the correct order of magnitude as the charge-order transition $T_m \sim 455$ K in the compound $\text{Na}_3\text{Cu}_2\text{O}_4$.⁸ Nevertheless we are far from any quantitative comparison, as 3D effects could lead to a further enhancement of T_m or to a reduction due to frustration effects resulting, e.g., from the interaction with Na-ion potentials.

Before we move on to the calculation of the optical conductivity, we briefly comment on the exact diagonalization scheme used. In the WL regime the eigenstates are energetically ordered according to the number of domain-wall pairs that are excited (c.f. Fig. 5). This property of the Coulomb interaction, i.e., that it removes the high degeneracy of the usual Hubbard model, allows us to truncate the Hilbert space by selecting configurations with a small number of domain walls, and to perform a full diagonalization in the truncated space defined by a cutoff energy. This procedure is expected to work well in the WL regime, but it should become less accurate in the CDW regime. As the CDW can be visualized rather as a Fermi sea with a small gap due to the relevant $2k_F$ scattering processes, a truncated domain-wall basis will certainly not be appropriate or require an extremely large cutoff energy such that again the full Hilbert space is covered. Figure 7(b) shows the convergency of the lowest excitation energies at $q=0$ and π as function of the cutoff energy. As can be seen from the figure, this truncation works extremely well even for $t_1=0.1$ V, i.e., at the crossover to the CDW regime. Thus most of our calculations for the bigger $N=26$ clusters employ an energy cutoff 1.45. Moreover a basis of momentum eigenstates is used to further reduce the size of the matrices.

C. Optical conductivity

Optical conductivity experiments could provide important information about the size of the charge gap, the presence or absence of exciton features, and the shape and width of the domain-wall continuum. Thus in combination with the theoretical spectra optical data may allow us to determine the basic parameters of the Hubbard-Wigner model more precisely. As we are dealing with insulating systems it suffices to focus on the finite frequency absorption $\sigma(\omega)$ as given by

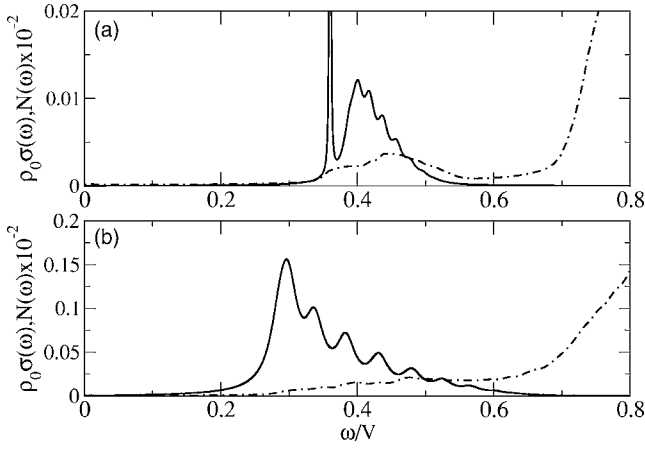


FIG. 9. Optical conductivity $\rho_0\sigma(\omega)$ at $T=0$ (solid line) and density of states $D(\omega)$ of two- and four-DW excitations (dashed line) for an $N=26$ chain with a Coulomb interaction for $t_1/V=0.02$ (top) and 0.05 (bottom), respectively. The spectra are shown with a Lorentzian broadening $\gamma=0.03$, while for the bound state in $\sigma(\omega)$ $\gamma=10^{-4}$ was used. The strong increase of $D(\omega)$ at $\omega\sim 0.7$ marks the onset of the four-DW continuum which does not contribute to $\sigma(\omega)$.

the Kubo equation in terms of the current-current correlation function⁶⁸

$$\sigma(\omega) = \frac{1 - e^{-\omega/T}}{N\omega} \text{Im} \sum_{m,n} \frac{e^{-E_m/T} \langle n | j_x | m \rangle^2}{\omega - (E_n - E_m) + i0^+}, \quad (20)$$

where $\langle n |$ ($|m\rangle$) are eigenstates with energy E_n (E_m), respectively. The current operator j_x for the lattice model is defined in the usual way as

$$j_x = - \sum_{i,l \geq 1} \delta_l t_l (c_i^\dagger c_{i+l} - c_{i+l}^\dagger c_i), \quad (21)$$

where $\delta_l = la$ is the hopping length, and a the Cu-Cu distance along the chain. The conductivity will be given in dimensionless form,⁶⁹ $\rho_0\sigma(\omega)$, with $\rho_0 = \hbar v / e^2 a^2$ where $v = abc$ is the cell volume per Cu site, and $\hbar / e^2 = 4.1 \text{ k}\Omega$ the von Klitzing constant.

In this section we consider nearest-neighbor-hopping amplitudes only. Equation (20) can be evaluated in a straightforward way via exact diagonalization. Results for $\sigma(\omega)$ at $T=0$ are given in Fig. 9 for two different hopping matrix elements $t_1/V = 0.02$ and 0.05 , which reveal the broadening of the domain-wall continuum $\sim 8t_1$ and the disappearance of the exciton peak at larger t_1 in the continuum. At $t_1=0.02 \text{ V}$ the exciton at energy 0.38 V has a large weight and the shape of the DW continuum is asymmetric and peaked at the lower frequency edge. The strong asymmetry of the continuum persists at larger t_1 , i.e., when the exciton is no longer visible. We stress that this strong asymmetry of the DW absorption is related to the domain-wall attraction in the Coulomb case, whereas in the model with truncated interaction ($l_{max}=1$) $\omega\sigma(\omega)$ turns out symmetric with respect to the center of the DW absorption.

Figure 9 also provides a comparison of $\sigma(\omega)$ with the total density of states:

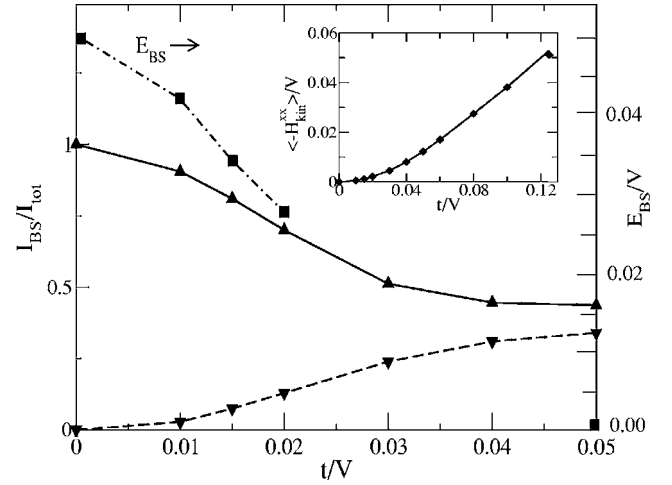


FIG. 10. Relative optical spectral weights of a bound state (solid line) and of the first continuum state (dashed) versus t_1/V calculated for an $N=26$ ring. The binding energy E_{BS} (squares) is given for small t_1 only because of the difficulty to extract this quantity from a discrete spectrum. The inset shows the kinetic energy (solid line) and the result obtained via the sum rule (triangles).

$$D(\omega) = (1/N) \sum_k \sum_n \delta(\omega - E_{k,n}). \quad (22)$$

The latter quantity shows a part of the two-domain wall continuum, which reaches up to $\omega \sim 0.6 \text{ V}$, also the much larger two particle-hole continuum involving four DW's. The latter, however, is not optically active. A comparison of $D(\omega)$ and $\sigma(\omega)$ indicates a strong enhancement of the optical matrix element towards the lower edge of the two DW continuum, i.e., leading to the asymmetric shape of $\sigma(\omega)$.

The weight of the lowest (exciton) excitation is compared in Fig. 10 with the weight of the second lowest excitation. It can be seen that the decay of exciton weight is rather fast with growing t_1 and parallel to the decrease of the exciton binding energy. The inset of Fig. 10 provides a comparison of the kinetic energy due to the quantum fluctuations and the integral over the optical conductivity as function of t_1 . The coincidence of the data reflects the optical sum rule⁷⁰

$$\frac{2}{\pi} \int_0^\infty d\omega \sigma(\omega) = \frac{1}{N} \sum_{l \geq 1} \delta_l^2 \langle -H_{kin}^l \rangle. \quad (23)$$

In the general case where different hopping processes in the kinetic energy H_{kin}^l , $l=1, 2, \dots$, reach over different distances δ_l the optical sum rule has to be modified and is given by an average over the individual kinetic energy contributions weighted by the square of the hopping distances.⁷¹ In all the cases considered thus far, the optical sum rule is fully exhausted by the incoherent part of $\sigma(\omega)$, thus there is no zero-frequency Drude contribution. The increase of the total spectral weight with t_1 naturally follows from the corresponding increase of kinetic energy. The quadratic dependence $\sim t_1^2/V$ at small t_1 highlights that the kinetic energy is due to virtual charge excitations with energy proportional to V .

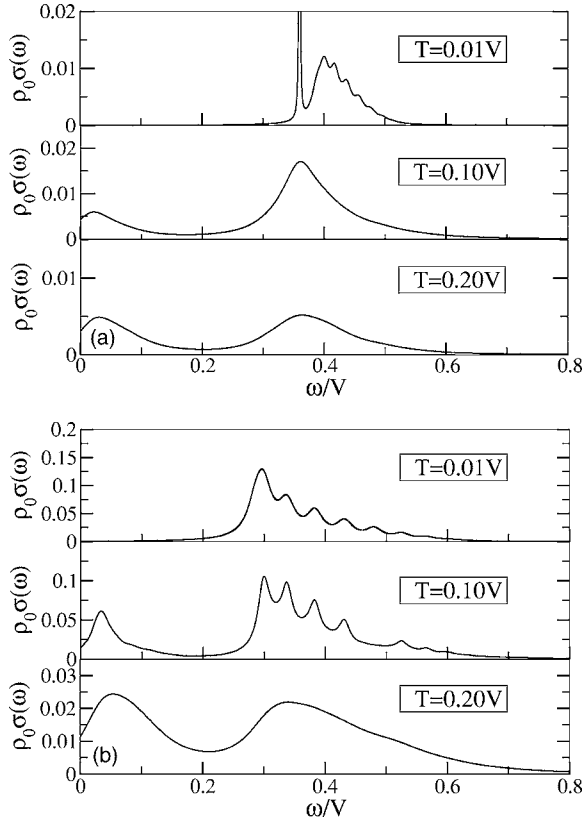


FIG. 11. Optical conductivity at quarter-filling ($\rho=0.5$): (a) $t_1=0.02$ V and (b) $t_1=0.05$ V for different temperatures $T=0.01, 0.10$, and 0.20 V.

Next we consider the thermal evolution of the optical conductivity spectra displayed in Fig. 11 for the two cases $t_1/V=0.02$ and 0.05 . The spectra shown were obtained for an $N=26$ site cluster and periodic boundary conditions. There are two immediately obvious features: (i) The disappearance of the prominent exciton absorption in the $t_1=0.02$ V case at high temperature, and (ii) the spectral weight transfer from high-energy into a low-energy gapless absorption. Furthermore one also realizes a gradual decrease of the total sum rule with increasing temperature.

The appearance of the low-energy absorption arises from the thermal population of excited states, i.e., exciton and continuum states, and subsequent transitions within the continuum. The evolution of the low-energy continuum dictates the temperature dependence of the dc conductivity. We shall come back to this point in Sec. VI.

IV. ROLE OF SECOND-NEIGHBOR HOPPING

Edge-sharing chain compounds have the peculiar property that the magnitude of the second-neighbor-hopping matrix element t_2 is larger than the nearest-neighbor matrix element t_1 . This has the important consequence that the Fermi surface topology is changed, i.e., instead of two Fermi points there can now be four Fermi points depending on the hole or electron concentration. Therefore we have here a qualitatively new situation compared to the pure t_1 case, where the modu-

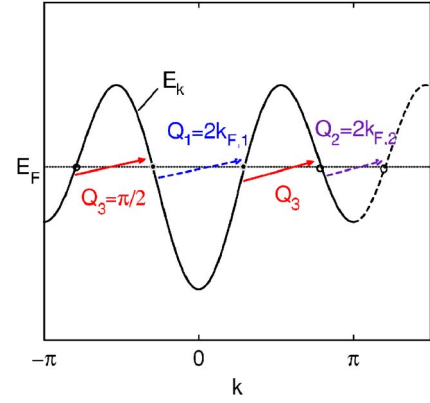


FIG. 12. (Color online) Free fermion dispersion E_k for $t_2/t_1=2.5$ with scattering processes $Q_1=2k_{F,1}$, $Q_2=2k_{F,2}$ and $Q_3=\pi/2$ (for $\rho=\frac{1}{2}$) indicated by arrows.

lations of the CDW arising from the Fermi surface instability and of the WL coincide. At sufficiently large values for t_2 , i.e., relative to the Coulomb interaction strength V , we expect the system to undergo a transition from the Wigner phase into a CDW state with different modulation, i.e., now dictated not by the classical Coulomb interaction but by “Fermi surface nesting,” that is a charge modulation of quantum mechanical origin.

For sufficiently large t_2 there are three relevant scattering processes $Q_1=2k_{F,1}$ and $Q_2=2k_{F,2}$ which are, in general, related to incommensurate modulations determined by the ratio t_2/t_1 , and a commensurate modulation $Q_3=\pi/2$ as shown in Fig. 12. Whereas Q_1 and Q_2 lead to the opening of gaps at two Fermi points, respectively, Q_3 generates gaps at all four Fermi points simultaneously. Our numerical results show that the Q_3 modulation is the dominant one, and leads to a further doubling of the unit cell. It is remarkable that the modulation Q_3 coincides with that of the $2k_F$ -Peierls instability at quarter-filling, that is in the usual model with nearest-neighbor hopping and spin. Here we shall not follow the weak-coupling route further, but investigate the transition to the CDW from the strong-coupling WL side.

It is immediately evident that in the perfect charge-ordered state t_2 processes are completely quenched, and only

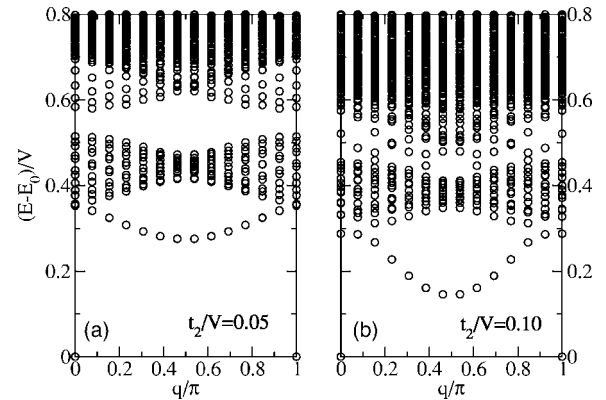


FIG. 13. Excitation spectrum for $N=26$, $t_1=0.02$ V and two different second-neighbor-hopping matrix elements $t_2=0.05$ and 0.10 V, showing the strong effect of t_2 on the exciton dispersion with a shift of the minimum to $q=\pi/2$.

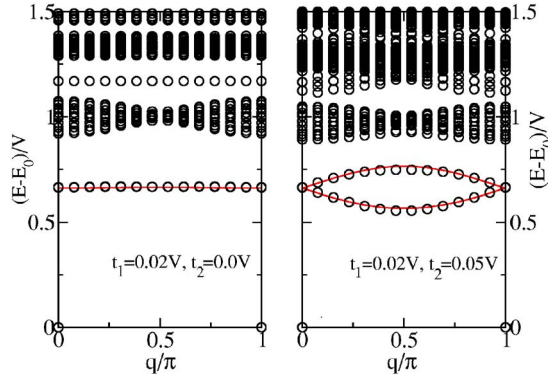


FIG. 14. (Color online) Excitation spectrum for an $N=26$ site ring at electron concentration $\rho=0.5$ and Coulomb interaction truncated at $l_{max}=3$. Numerical results (circles) for $t_1=0.02$ V and two different second-neighbor-hopping matrix elements: (a) $t_2=0$ and (b) 0.05 V. Analytical results for domain-wall exciton states are shown as solid lines.

through the presence of charge fluctuations introduced via nearest-neighbor hopping t_1 the t_2 processes are activated. This is seen in the excitation spectra for the Coulomb chain shown in Figs. 13. The exact diagonalization results show even for $t_2=0.10$ hardly any effect on the two-DW continuum. A small downward shift of the two-DW spectrum is attributed to a broadening of the four DW continuum.

The exciton, however, is changed in a surprising way; it disperses downward, in contrast to the t_1 case studied before. The numerical solution reveals two further aspects: (i) the periodicity of the exciton dispersion indicates nearest-neighbor hopping of DW's, quite in contrast to the t_1 motion where DW's hop over two sites; and (ii) the exciton dispersion does not depend on the sign of t_2 .

For further illustration we present in Fig. 14 exact diagonalization results for the excitation spectrum of the model with an interaction truncated at $l_{max}=3$. The domain wall interaction in this case is $\Delta_1=\frac{2}{3}V$ and $\Delta_m=\Delta_2=V$ for $m \geq 2$. The DW continuum is centered around V . The dispersion of the exciton in case (a) with $t_1=0.02$ V and $t_2=0$ is strongly suppressed as compared to the case with long-range Coulomb interaction (cf. Fig. 5). As we shall see below, this is due to the larger splitting $\Delta_2-\Delta_1$ between the exciton and the continuum as compared to the model with Coulomb interaction.

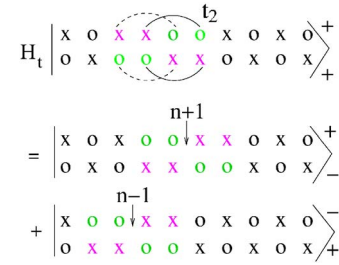


FIG. 15. (Color online) Sketch of second-neighbor t_2 hopping processes between energetically degenerate and symmetrized DW configurations. Such processes occur only in the $m=1$ sector between symmetric and antisymmetric configurations (due to the Pauli principle) and lead to a nearest-neighbor motion of the center of mass of the DW pair. Signs attached to the right brackets indicate even and odd linear combinations.

At finite $t_2=0.05$ [Fig. 14(b)] the degeneracy of the exciton is lifted and one observes clearly two exciton branches, one with downward and one with upward dispersion. To get some deeper insight in the peculiar dispersion of the exciton at finite t_2 , we turn now to the analytical analysis of the excitonic state for the latter case, i.e., defined by the DW potential $\Delta_1=\frac{2}{3}V$ and $\Delta_m=V$ for $m \geq 2$.

A. Analytical study of the exciton state

The analytical calculations presented in Sec. III A can be extended to the case with a finite next-nearest-neighbor-hopping term. For $\rho=\frac{1}{2}$ t_2 -hopping processes are completely blocked in the ground state with a perfect charge order. A nearest-neighbor DW pair, however, can move by one step to the left or to the right as a result of a t_2 process as indicated in Fig. 15. For the analytical solution it is useful to adopt symmetrized configurations as shown in Fig. 15.

There are only relevant matrix elements $\sim t_2$ between even and odd configurations in the $m=1$ sector that are energetically degenerate:

$$-\langle \psi_{q,1} | H_{t_2} | \psi_{q,1} \rangle_+ = t_2(q), \quad (24)$$

where $t_2(q)=2it_2\sin(q)$. This matrix element connects the even and odd sectors in the secular determinant:

$$D = \begin{vmatrix} \ddots & \ddots & 0 & \dots & \dots & \dots & 0 \\ t_1(q) & \omega_2 & t_1(q) & 0 & \dots & \dots & 0 \\ 0 & t_1(q) & \omega_1 & t_2(q) & 0 & \dots & 0 \\ 0 & \dots & t_2^*(q) & \omega_1 & t_1(q) & 0 & 0 \\ 0 & \dots & 0 & t_1(q) & \omega_2 & t_1(q) & 0 \\ 0 & \dots & 0 & 0 & t_1(q) & \omega_2 & \ddots \\ 0 & \dots & 0 & 0 & \ddots & \ddots & \ddots \end{vmatrix}. \quad (25)$$

The expansion of the secular determinant yields a modified equation for the bound states

$$[\omega_1 p - t_1(q)^2]^2 - |t_2(q)|^2 p^2 = 0. \quad (26)$$

The t_2 term leads to a splitting of the degenerate solutions obtained in the t_1 case into a lower and an upper branch:

$$E_{ex,l}(q) = \Delta_1 - |t_2(q)| - \frac{t_1(q)^2}{\Delta_2 - \Delta_1 + |t_2(q)|}, \quad (27)$$

$$E_{ex,u}(q) = \Delta_1 + |t_2(q)| - \frac{t_1(q)^2}{\Delta_2 - \Delta_1 - |t_2(q)|}. \quad (28)$$

The coupling t_2 shifts the exciton minimum in the lower branch to $\pi/2$. The exciton dispersion does not depend on the relative sign of t_2 . At a threshold value $t_{2,cr}$ $q = \pi/2$ excitons condense and lead to the new state controlled by the kinetic energy. The upper branch is a physical solution only as long as it does not touch the DW continuum.

In Fig. 14 we provide a comparison of the analytical solutions for the exciton dispersions, Eqs. (27) and (28), with exact diagonalization data for an $N=26$ site cluster in the case of the Coulomb interaction truncated at $l_{max}=3$. As can be seen from Fig. 4 in this case $\Delta_1 = \frac{2}{3}V$ and $\Delta_m = \Delta_2 = V$ for $m \geq 2$. The analytical exciton dispersions calculated from Eqs. (27) and (28) provide a good description of the numerical values. The small deviations are mainly due to a slight downward shift of the two-DW continuum in the numerical calculation, that results from its interaction with the four-DW continuum which is much broader in the $t_2=0.05$ case. This also implies a small downward shift of the DW exciton.

It is also instructive to compare Fig. 14(b) calculated for the truncated interaction to Fig. 13(a) which was obtained using the full Coulomb interaction. In the latter case only the lower exciton branch can be seen and its dispersion is slightly larger than in Fig. 14(b), although the spectra have been determined for the same hopping parameters. These differences result from the different attraction of domain walls $\Delta_2 - \Delta_1$ in the two cases, which enter in the third term on the rhs of exciton dispersion in Eq. (27).

The critical value $t_{2,cr}$ can be estimated from Eq. (27) by setting $E_{ex,l}(q)=0$ at $q = \pi/2$. For the case with long-range Coulomb interaction (cf. Fig. 13) we use the parametrization $\Delta_1/V = 2 \ln 2 - 1$ and $\Delta_m/V = \frac{1}{2}$ for $m \geq 2$. This yields $t_{2,cr} \sim 0.18$ V, i.e., somewhat larger than the numerical value $t_{2,cr} = 0.155$ V obtained by an exact diagonalization of an $N=26$ site cluster. One reason for the overestimate is obvious from Fig. 13 which shows a broadening of the four DW continuum at large t_2 , i.e., leading to a downward shift of the two DW continuum and thereby to a smaller $t_{2,cr}$.

B. Structure factor and exciton instability

In the previous discussion of the electronic structure we have seen that the exciton will get soft at about $t_2 = 0.16$ V and hence the WL state should get unstable and a new ground state with a momentum $q \sim \pi/2$ should appear. In the following we analyze the change of the static charge structure factor $N(q)$. Figure 16 shows the dependence of $N(q)$,

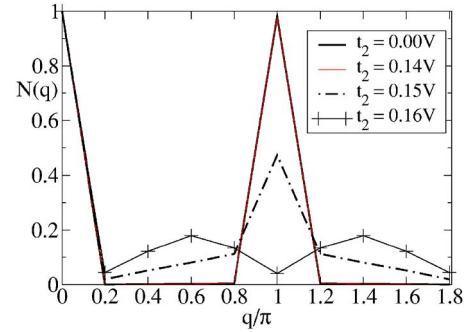


FIG. 16. (Color online) Charge structure factor $N(q)$ as obtained by ED for a 10 site ring with Coulomb interaction ($V=1$) and $\rho=0.5$ for $t_1=0.02$ and different values for t_2 ($T=0.01$ V). Straight lines are guides to the eyes; the + symbols in the data for $t_2=0.16$ also indicate the allowed q points. The Wigner order is unstable beyond the critical value $t_2^{cr}=0.155$.

Eq. (19), on the size of t_2 for fixed $t_1=0.02$ V. The results are obtained for an $N=10$ site cluster where we included the full Hilbert space in order to show the complete break-down of Wigner order at large t_2 .

It is remarkable that up to the value $t_2 \leq 0.14$ the ground state correlations remain unchanged with $N(q)$ peaked at momentum π . This reflects the blocking of t_2 hopping processes in the state with an alternating charge order. Then in the narrow range $0.15 > t_2 > 0.16$ there is a sudden change of $N(q)$ indicating a level crossing. Beyond $t_2 \sim 0.16$ the charge correlations are determined by the new state with the maximum of $N(q)$ near $\pi/2$. The broad shape of $N(q)$ is reminiscent of that of a 1D Fermi gas, i.e., indicating that the CDW modulations in this phase are rather weak. It has been checked by a calculation of the charge correlation functions in real space, that there are still significant charge modulations in the system consistent with a $q = \pi/2$ CDW.

The excitation spectrum corresponding to the transition from the WL to the $\pi/2$ CDW is shown in Fig. 17(a). It clearly reveals the quasidegeneracy of the WL ground states at $q=0(\pi)$ and the soft exciton at $q = \pi/2$. At larger values for t_2 the state emerging from the exciton is the

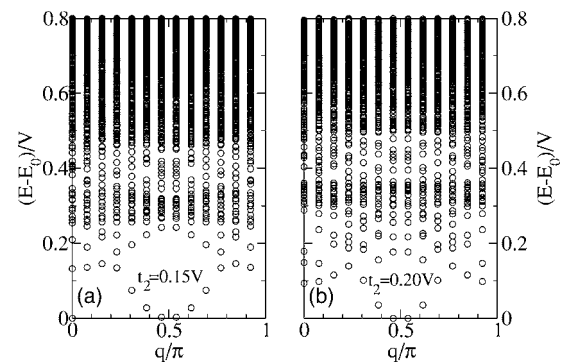


FIG. 17. Excitation spectrum for $L=26$, $t_1=0.02$ V and two different second-neighbor-hopping matrix elements $t_2=0.15$ and 0.20 V indicating the exciton instability of the Wigner lattice. While for $t_2=0.15$ the degenerate ground states are at $q=0, \pi$, the ground state momenta for $t_2=0.20$ are near $q = \pi/2$.

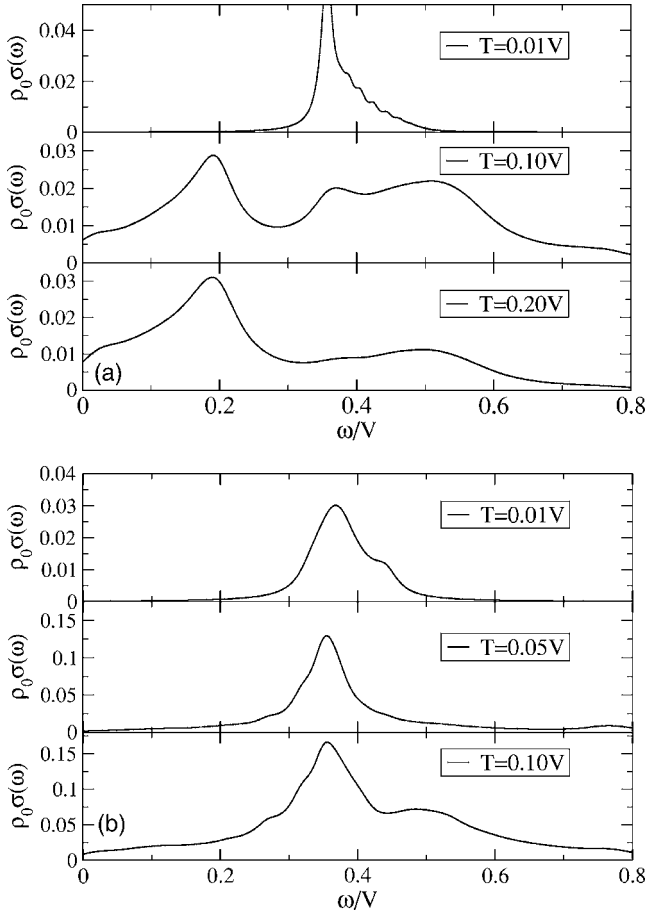


FIG. 18. Optical conductivity at quarter-filling ($\rho=0.5$) for different temperatures: (a) $t_1=0.02, t_2=0.05$ (Lorentzian broadening $\gamma=0.05$ V), and (b) $t_1=0.02, t_2=0.10$. The in-gap absorption appearing near $\omega \sim 0.19$ V at finite temperatures in (a) is attributed to a transition from the thermally excited exciton in the vicinity of $q=\pi$ to the domain-wall continuum. A similar feature appears in (b) at $\omega \sim 0.27$ V.

new ground state of the system, as seen in Fig. 17(b). We note, that our program was developed for $N=4n+2$ site rings ($n=1, 2, \dots$) that do not have $\pi/2$ as allowed momentum, therefore there are two degenerate ground states at $q=\pi/2 \pm 2\pi/N$.

C. Optical conductivity

The effect of second-neighbor hopping t_2 on the optical conductivity $\sigma(\omega)$ is displayed in Figs. 18(a) and 18(b) for the model with Coulomb interactions. As a consequence of the blocking of t_2 processes in the state with alternating Wigner charge order at $\rho=\frac{1}{2}$ the optical spectra are only slightly modified at low temperature, and almost coincide with those obtained for the model with only nearest-neighbor hopping in Fig. 11. A remarkable change, however, is the disappearance of the $q=0$ exciton, which was very pronounced in the spectrum for $t_1=0.02$ and $t_2=0$ in Fig. 11(a) at low temperature. This feature has disappeared after switching on $t_2=0.05$ in Fig. 18(a). For these parameters there is no bound state at $q=0(\pi)$ as can also be seen from

the corresponding energy level diagram in Fig. 13(a).

As an optical experiment involves only vertical transitions only charge excitations at $q=0$ and π are probed at low temperature, i.e., the downward dispersing exciton is invisible. This changes, however, when the exciton states get populated by thermal excitations. As a consequence there are marked changes in the spectra at higher temperature, which can be traced back to the different dispersion of the exciton state at finite t_2 . The pronounced structure near $\omega=0.2$ in Fig. 18(a) at $T=0.1$ V, which is already seen at $T=0.05$ V as a weak *in-gap excitation*, stems from transitions between thermally excited excitons near $q=\pi/2$ and final states at the upper edge of the two DW continuum [cf. Fig. 13(a)]. This conclusion is based on a careful study of the size of the corresponding matrix elements in the current-current correlation function. In the spectra of Fig. 18(b) for a twice as large t_2 value this absorption has shifted to higher energies ($\omega \sim 0.27$ V) and appears now as a small structure on the shoulder of the main peak, which is due to transitions into the two DW continuum at $q=0$.

Thus the observation of an in-gap absorption in the optical conductivity at finite temperature can provide valuable information about the position of the minimum of the exciton dispersion in the middle of the Brillouin zone, which may allow us to determine the value of t_2 from experiment.

Finally we recall that the higher transitions into the upper Hubbard band with energy $\sim U$ are not contained in the spinless fermion model we study here. Yet they are contained in the Hubbard-Wigner model. For $t_2 \geq t_1$ and $\rho=\frac{1}{2}$ these transitions are expected at energy $U-V_2$ with intensity $\sim t_2^2$. But also in the case $t_2 \ll t_1$ transitions into the upper Hubbard band are expected due to charge fluctuations resulting from t_1 processes.

V. dc CONDUCTIVITY

A central experimental quantity to compare our finite temperature results with is certainly the dc conductivity $\sigma(T)$. In Fig. 11, which displays the temperature dependence of $\sigma(\omega)$, we observe the emergence of a low-frequency continuum whose intensity grows with increasing temperature. These changes are accompanied by a spectral weight transfer from a high to low energy. The low-energy excitations arise from transitions within the two DW continuum. We note that at higher temperatures, i.e., near the melting temperature of the WL and above, also four DW excitations do contribute substantially to the low-frequency absorption. This yields a very dense low-energy spectrum even for small systems. It is certainly suggestive that this low-frequency continuum contains the information about the dc conductivity. Yet as we are dealing with finite systems the case is not that simple as the zero-frequency limit cannot be determined in a straightforward way. In fact, the analysis of the low-frequency part of $\sigma(\omega)$ reveals a pseudogap $\sim 8t_1/N$, which scales inversely with the size of the system N .

Similar pseudogap behavior and finite size effects in $\sigma(\omega)$ have also been observed recently by Prelovsek *et al.*⁷² in a study of the 1D t - V model. In their careful study Prelovsek *et al.* arrived at the conclusion that after finite size scaling the

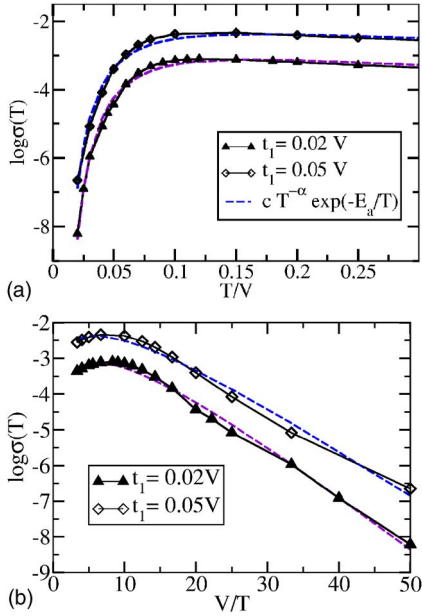


FIG. 19. (Color online) (a) Temperature dependence of the dc conductivity for $\rho=0.5$ determined from the integrated low-frequency spectral weight for $t_1=0.02$ and 0.05 ($t_2=0$). (b) Arrhenius plot revealing the activated behavior at low temperature. An activated behavior for the carrier density in combination with a temperature dependent mobility $\sim T^{-\alpha}$, Eq. (30), provides a rather good fit of the numerical data over the whole temperature range.

results for the frequency dependence could be compatible with a normal and featureless shape of $\sigma(\omega)$ as found by a frequency moment analysis.

Thus we proceed as follows: We assume that in the thermodynamic limit the level spacing vanishes and the low-frequency part of the spectrum can be expressed by a Drude form for the real part of the conductivity $\sigma(\omega) = \sigma(T) / [1 + (\omega\tau)^2]$, where $\tau \approx 1/t_1$ is determined by the energy scale of the domain-wall continuum. The spectral weight of the low-frequency part of $\sigma(\omega)$ as determined by exact diagonalization

$$I(\omega_0) = \int_0^{\omega_0} \sigma(\omega) d\omega, \quad (29)$$

with $\omega_0 = 4t_1$ is then used to determine the dc conductivity $\sigma(T)$.

Results for the dc conductivity obtained from a 26 site ring at doping $\rho=0.5$ are presented in Fig. 19 for two different hopping matrix elements. The numerical data for $t_1=0.02$ and 0.05 V ($t_2=0$) show similar behavior. The dc conductivity reveals activated behavior below and basically T -independent (poor metallic) behavior above the melting temperature T_m of the WL. The conductivity for $t_1=0.02$ V is smaller, reflecting the t_1^2 proportionality of the current-current correlation function.

At a small hopping $t_1=0.02$ V the numerical data for $\sigma(T)$ is well described over five decades by a single activation energy dependence $\sigma(T) \approx c \exp(-E_a/kT)$, with $E_a \approx 0.30$ V. However, the sometimes used relation^{73,74}

$$\sigma(T) \approx c T^{-\alpha} \exp(-E_a/kT), \quad (30)$$

which involves in addition the temperature dependence of the mobility $\mu(T) \sim T^{-\alpha}$, improves the fit when approaching the saturation (melting) regime at high temperature as shown in Fig. 19 by dashed lines. Using this relation we obtained for $t_1=0.02(0.05)$ V the activation energies $E_a \sim 0.39(0.32)$ V, respectively, and $\alpha \sim 2.4(1.95)$. Thus the mobility $\mu(T)$ of the carriers (domain walls) decreases strongly with increasing temperature, as one may have expected. The activation energies E_a determined from $\sigma(T)$ are consistent with the energy gaps in the corresponding energy level diagrams in Figs. 5(a) and 5(b). Yet the activation energies E_a determined from $\sigma(T)$ are larger than expected from the relation $E_a = E_g/2$ which applies for usual semiconductors. Whether this discrepancy originates from the fact that the charge carriers in the WL are domain walls with a fractional charge and not usual electronlike and holelike quasiparticles remains unclear and deserves further study.

While the relation Eq. (30) provides a quite satisfactory description of the numerical data over the full temperature range, it is nevertheless far from perfect. As one can see, the fit curve in Fig. 19(b) lies below (above) the numerical data for temperatures above (below) the melting temperature T_m , respectively. This deviation possibly reflects the strong change of the structure factor near T_m (see inset of Fig. 8). Here our aim was to keep the number of parameters as small as possible and therefore we have not tried to add such a $E_a(T)$ correction term that would involve T_m and further parameters.

Recent measurements of the dc conductivity of $\text{Na}_3\text{Cu}_2\text{O}_4$ and $\text{Na}_8\text{Cu}_5\text{O}_{10}$ compounds show the same trends: (i) an Arrhenius behavior below, and (ii) a saturation of dc conductivity above the melting transition $T_m \sim 455(540)$ K, respectively.^{8,75} Moreover, the experimental conductivities show only a small discontinuity at the melting temperature T_m . Although the absence of a discontinuity in the theoretical curve can be attributed to the finite system, which is not expected to display a phase transition, it is nevertheless remarkable that also the experimental data only show a weak discontinuity at the melting temperature T_m of the WL. The measured dc conductivity of the compound $\text{Sr}_{14}\text{Cu}_{24}\text{O}_{41}$ was also found to be described by an Arrhenius law with an activation energy $E_a \sim 0.12$ eV. More recent studies found a crossover between two exponential regimes, with $E_a \sim 0.12$ eV for the low T regime up to about 170 K but different values 0.18 eV,¹⁶ 0.22 eV,⁷⁶ and 0.27 eV (Ref. 77) for the high- T regime. Up to 400 K no saturation was observed for this compound. As the transport at high temperatures is probably due to the chains and the ladders in these compounds, a direct comparison with our results is ruled out.

VI. CONCLUSIONS

In summary, we have investigated the charge excitations of a 1D generalized Wigner lattice, expected to be realized in edge-sharing Cu-O chain systems and also in some organic chain compounds, starting from the Hubbard-Wigner model with long-range Coulomb interactions $V_l = V/|l|$ among elec-

trons. A central aim was to gain insight into the spectral structure of the optical conductivity $\sigma(\omega)$ and its temperature dependence.

We have found the following:

(i) The conductivity $\sigma(\omega)$ is determined by a highly asymmetric spectrum due to two domain-wall excitations with an energy gap $E_g \sim V/2 - 4t_1$ and a width of $\sim 8t_1$. The asymmetric form of this spectrum may serve as another fingerprint to detect the WL and may also be employed to determine the parameters of the model from experiment.

(ii) For $t_1 \ll V$ excitons with a dispersion given by Eq. (18) form and show up as strong absorption peaks in the optical conductivity. The excitons are due to an attractive potential between domain-wall pairs $\sim V/8l$, whose prefactor reflects the fractional charge of the DW. The DW attraction results as a consequence of the long-range (repulsive) Coulomb interaction between electrons. The appearance of excitonic states, which arise from the effective attraction between the fractionally charged DW's, was, to our knowledge, not noted before. In contrast, the frequently studied model with only nearest-neighbor interactions has no bound state because of the absence of attractive interactions between DW pairs. However, in that case interchain interactions may provide an alternative mechanism for confinement, as noted recently in work by Bhaseen and Tselik.⁶⁰

(iii) Edge-sharing chain compounds have the unusual property that the magnitude of the second-neighbor-hopping matrix element t_2 is larger than the nearest-neighbor matrix element t_1 . While t_2 hopping processes are frustrated in the classical WL state with alternating charge order, these processes surprisingly contribute strongly to the exciton dispersion. They lift the degeneracy of the exciton state and the lower branch, c.f. Eq. (27), leads to an exciton instability at about $t_{2,c} \sim 0.155 V$. The CDW state beyond $t_{2,c}$ has a modulation period twice as large as that of the WL. The charge modulation is weak in this CDW state as inferred from the calculation of the static charge structure factor.

(iv) Interestingly the optical conductivity at a finite temperature reveals an in-gap absorption that reflects the transi-

tions between the soft exciton near $q = \pi/2$ and the domain-wall continuum. Thus this in-gap absorption may provide a further identification of the WL state and also allow us for an independent experimental determination of the matrix element t_2 .

(v) Moreover, we have calculated the temperature dependence of the dc conductivity of the generalized Wigner lattice from the low-frequency absorption. The data for $\sigma(T)$ show a crossover from activated behavior at low temperature to a basically temperature independent (poor metal-like) conductivity at high temperatures. It turns out that $\sigma(T)$ can be described over the full temperature range by an activated behavior characterized by an activation energy E_a and a temperature dependent mobility $\sim T^{-\alpha}$. This implies a strong decrease of the mobility of domain walls with increasing temperature.

Finally we note that doped edge-sharing compounds provide a unique opportunity to study the competition between two entirely different states, the classical WL dictated by the long-range Coulomb interaction and the CDW of quantum mechanical origin, i.e., resulting from a Fermi surface instability. These materials highlight the importance of long-range Coulomb interaction in strongly correlated systems, and provide a one-dimensional test ground for the study of charge stripe formation. We have analyzed here the charge dynamics and aspects of transport for a generalized 1D Wigner lattice in its most simple realization, namely at quarter-filling ($\rho = \frac{1}{2}$). Other commensurabilities are more complex and show a hierarchy of different charge excitations. Work along these lines is in progress, as well as work on the effect of spin-charge coupling particularly on the low-energy charge response.

ACKNOWLEDGMENTS

We like to thank M. Jansen, G. Khaliullin, B. Keimer, W. Metzner, A. Mishra, and R. Zeyher for useful discussions, and M. Daghofer for discussions and helpful comments on the manuscript.

*Present address: Department of Physics, University of Tennessee, Knoxville, TN 37996, and Condensed Matter Sciences Division, Oak Ridge National Laboratory, Oak Ridge, TN 37381. USA.

¹E. Wigner, Phys. Rev. **46**, 1002 (1934).

²J. Hubbard, Phys. Rev. B **17**, 494 (1978).

³J. Kondo and K. Yamaji, J. Phys. Soc. Jpn. **43**, 424 (1977).

⁴V. J. Emery, Phys. Rev. Lett. **37**, 107 (1976).

⁵J. E. Hirsch and D. J. Scalapino, Phys. Rev. B **29**, 5554 (1984).

⁶H. J. Schulz, Phys. Rev. Lett. **71**, 1864 (1993).

⁷For an electron concentration $\rho = m/n$, the WL unit cell size is n lattice units, as for a $4k_F$ CDW with density modulation $\rho(l) = \rho_0 + \rho_1 \cos(4k_F l)$ and $4k_F = 2\pi m/n$.

⁸P. Horsch, M. Sofin, M. Mayr, and M. Jansen, Phys. Rev. Lett. **94**, 076403 (2005).

⁹M. Sofin, E.-M. Peters, and M. Jansen, J. Solid State Chem. **178**, 3708 (2005).

¹⁰Instead of k_F there are now two Fermi momenta $k_{F,1}$ and $k_{F,2}$, which depend on the electron concentration and on the ratio t_2/t_1 .

¹¹George Grüner, *Density Waves in Solids* (Addison-Wesley, Reading, 1994).

¹²A quantum solid is intrinsically restless in the sense that atoms continuously vibrate about their position *and* exchange places even at an absolute zero temperature. In the case of WL atoms are replaced by electrons.

¹³E. Polturak and N. Gov, Contemp. Phys. **44**, 145 (2003).

¹⁴M. W. McElfresh, J. M.D. Coey, P. Strobel, and S. von Molnar, Phys. Rev. B **40**, 825 (1989).

¹⁵T. Osafune, N. Motoyama, H. Eisaki, and S. Uchida, Phys. Rev. Lett. **78**, 1980 (1997).

¹⁶G. Blumberg, P. Littlewood, A. Gozar, B. S. Dennis, N. Motoyama, H. Eisaki, and S. Uchida, Science **297**, 584 (2002).

- ¹⁷E. M. McCarron, M. A. Subramanian, J. C. Calabrese, and R. L. Harlow, *Mater. Res. Bull.* **23**, 1355 (1988).
- ¹⁸E. Dagotto and T. M. Rice, *Science* **271**, 618 (1996).
- ¹⁹U. Ammerahl, B. Büchner, L. Colonescu, R. Gross, and A. Revcolevschi, *Phys. Rev. B* **62**, 8630 (2000).
- ²⁰S. A. Carter, B. Batlogg, R. J. Cava, J. J. Krajewski, W. F. Peck, Jr., and T. M. Rice, *Phys. Rev. Lett.* **77**, 1378 (1996).
- ²¹R. Klingeler, N. Tristan, B. Büchner, M. Hücker, U. Ammerahl, and A. Revcolevschi, *Phys. Rev. B* **72**, 184406 (2005).
- ²²T. Fukuda, J. Mizuki, and M. Matsuda, *Phys. Rev. B* **66**, 012104 (2002).
- ²³Y. Gotoh, I. Yamaguchi, Y. Takahashi, J. Akimoto, M. Goto, M. Onoda, H. Fujino, T. Nagata, and J. Akimitsu, *Phys. Rev. B* **68**, 224108 (2003).
- ²⁴S. van Smaalen, *Phys. Rev. B* **67**, 026101 (2003).
- ²⁵M. Braden, J. Etrillard, A. Gukasov, U. Ammerahl, and A. Revcolevschi, *Phys. Rev. B* **69**, 214426 (2004).
- ²⁶A. Gellé and M.-B. Lepetit, *Phys. Rev. Lett.* **92**, 236402 (2004).
- ²⁷M. Isobe, M. Onoda, T. Ohta, F. Izumi, K. Kimoto, E. Takayama-Muromachi, A. W. Hewat, and K. Ohoyama, *Phys. Rev. B* **62**, 11667 (2000).
- ²⁸P. Abbamonte, G. Blumberg, A. Ruydi, A. Gozar, P. G. Evans, T. Siegrist, L. Venema, H. Eisaki, E. D. Isaacs, and G. A. Sawatzky, *Nature (London)* **431**, 1078 (2004).
- ²⁹P. Fazekas, *Electron Correlation and Magnetism* (World Scientific, Singapore, 1999).
- ³⁰J. B. Goodenough, *Phys. Rev.* **100**, 564 (2003).
- ³¹J. Bala and P. Horsch, *Phys. Rev. B* **72**, 012404 (2005).
- ³²R. H. McKenzie, J. Merino, J. B. Marston, and O. P. Sushkov, *Phys. Rev. B* **64**, 085109 (2001).
- ³³M. Calandra, J. Merino, and R. McKenzie, *Phys. Rev. B* **66**, 195102 (2002).
- ³⁴M. Dressel, N. Drichko, J. Schlueter, and J. Merino, *Phys. Rev. Lett.* **90**, 167002 (2003).
- ³⁵A. Greco, J. Merino, A. Foussats, and R. H. McKenzie, *Phys. Rev. B* **71**, 144502 (2005).
- ³⁶J. M. Tranquada *et al.*, *Nature (London)* **375**, 561 (1995).
- ³⁷F. C. Zhang and T. M. Rice, *Phys. Rev. B* **37**, 3759 (1988).
- ³⁸For the $\text{Na}_{1+x}\text{CuO}_2$ compounds the density $\rho=x$.
- ³⁹In the case of periodic boundary conditions $V_l = \max[V/l, V/(N-l)]$, where $1 \leq l \leq N-1$.
- ⁴⁰Y. Mizuno, T. Tohyama, S. Maekawa, T. Osafune, N. Motoyama, H. Eisaki, and S. Uchida, *Phys. Rev. B* **57**, 5326 (1998).
- ⁴¹R. Weht and W. E. Pickett, *Phys. Rev. Lett.* **81**, 2502 (1998).
- ⁴²L. Capogna, M. Mayr, P. Horsch, M. Raichle, R. K. Kremer, M. Sofin, A. Malyuk, M. Jansen, and B. Keimer, *Phys. Rev. B* **71**, 140402(R) (2005).
- ⁴³K.-Y. Choi, V. P. Gnezdilov, P. Lemmens, L. Capogna, M. R. Johnson, M. Sofin, M. Maljuk, M. Jansen, and B. Keimer, *Phys. Rev. B* **73**, 094409 (2006).
- ⁴⁴M. Horvatic, C. Berthier, F. Tedoldi, A. Comment, M. Sofin, M. Jansen, and R. Stern, *Prog. Theor. Phys.* **159**, 106 (2005).
- ⁴⁵J. Schnack, *Eur. Phys. J. B* **45**, 311 (2005).
- ⁴⁶M. Matsuda, K. Katsumata, H. Eisaki, N. Motoyama, S. Uchida, S. M. Shapiro, and G. Shirane, *Phys. Rev. B* **54**, 12199 (1996).
- ⁴⁷R. Klingeler, B. Büchner, K.-Y. Choi, V. Kataev, U. Ammerahl, A. Revcolevschi, and J. Schnack, *Phys. Rev. B* **73**, 014426 (2006).
- ⁴⁸E. H. Lieb and F. Y. Wu, *Phys. Rev. Lett.* **20**, 1445 (1968).
- ⁴⁹H. J. Schulz, G. Cuniberti, and P. Pieri, cond-mat/9807366 (unpublished).
- ⁵⁰J. M. P. Carmelo and P. Horsch, *Phys. Rev. Lett.* **68**, 871 (1992); J. M. P. Carmelo, P. Horsch, and A. A. Ovchinnikov, *Phys. Rev. B* **45**, 7899 (1992); J. M. P. Carmelo, P. Horsch, and A. A. Ovchinnikov, *ibid.* **46**, 14728 (1992).
- ⁵¹W. Stephan and P. Horsch, *Phys. Rev. B* **42**, 8736 (1990); P. Horsch and W. Stephan, *ibid.* **48**, 10595 (1993).
- ⁵²T. Giamarchi, *Quantum Physics in One Dimension* (Clarendon Press, Oxford, 2004).
- ⁵³T. Tohyama, P. Horsch, and S. Maekawa, *Phys. Rev. Lett.* **74**, 980 (1995).
- ⁵⁴S. Fratini, B. Valenzuela, and D. Baeriswyl, *Synth. Met.* **141**, 193 (2004); B. Valenzuela, S. Fratini, and D. Baeriswyl, *Phys. Rev. B* **68**, 045112 (2003).
- ⁵⁵H. DeRaedt and A. Lagendijk, *Phys. Rev. B* **27**, 921 (1983).
- ⁵⁶Y. Hatsugai, *Phys. Rev. B* **56**, 12183 (1997).
- ⁵⁷K. Penc and F. Mila, *Phys. Rev. B* **49**, 9670 (1994).
- ⁵⁸R. T. Clay, S. Mazumdar, and D. K. Campbell, *Phys. Rev. B* **67**, 115121 (2003).
- ⁵⁹D. Poilblanc, S. Yunoki, S. Maekawa, and E. Dagotto, *Phys. Rev. B* **56**, R1645 (1997).
- ⁶⁰M. J. Bhaseen and A. M. Tselik, cond-mat/0409602 (unpublished).
- ⁶¹S. Capponi, D. Poilblanc, and T. Giamarchi, *Phys. Rev. B* **61**, 13410 (2000).
- ⁶²N. D. Mermin and H. Wagner, *Phys. Rev. Lett.* **17**, 1133 (1966).
- ⁶³P. Bruno, *Phys. Rev. Lett.* **87**, 137203 (2001).
- ⁶⁴F. J. Dyson, *Commun. Math. Phys.* **12**, 91 (1969).
- ⁶⁵S. C. Erwin and C. S. Hellberg, *Surf. Sci. Lett.* **585**, L171 (2005).
- ⁶⁶As in the generalized Wigner lattice electrons are confined to one dimension, melting is not associated with the vanishing of the shear force but rather with the disappearance of long-range correlations.
- ⁶⁷We associate the melting temperature T_m *ad hoc*, but consistent with the study of Ref. 65, with a 10% reduction of the structure factor $N(q=\pi)$ compared to its zero temperature value.
- ⁶⁸G. D. Mahan, *Many-Particle Physics* (Plenum Press, New York, 1990).
- ⁶⁹F. Mack and P. Horsch, *Phys. Rev. Lett.* **82**, 3160 (1999).
- ⁷⁰D. Baeriswyl, J. Carmelo, and A. Luther, *Phys. Rev. B* **33**, 7247 (1986).
- ⁷¹M. Aichhorn, P. Horsch, W. von der Linden, and M. Cuoco, *Phys. Rev. B* **65**, 201101 (2002).
- ⁷²P. Prelovšek, S. El Shawish, X. Zotos, and M. Long, *Phys. Rev. B* **70**, 205129 (2004).
- ⁷³A. J. Epstein, E. M. Conwell, D. J. Sandman, and J. S. Miller, *Solid State Commun.* **23**, 355 (1977).
- ⁷⁴R. P. McCall, D. B. Tanner, J. S. Miller, and A. J. Epstein, *Phys. Rev. B* **35**, 9209 (1987).
- ⁷⁵M. Sofin, *Neue Alkalioxometallate über die Azid/Nitrat Route*, thesis, University Stuttgart, 2003.
- ⁷⁶A. Maeda, R. Inoue, H. Kitano, N. Motoyama, H. Eisaki, and S. Uchida, *Phys. Rev. B* **67**, 115115 (2003).
- ⁷⁷B. Gorshunov, P. Haas, T. Room, M. Dressel, T. Vuletić, B. Korin-Hamzić, S. Tomić, J. Akimitsu, and T. Nagata, *Phys. Rev. B* **66**, 060508(R) (2002).